Numerical simulation of lid driven flow in a curved corrugated porous cavity filled with *CuO*-water in the presence of heat generation/absorption

Syed S. Shah [a], Rizwan ul Haq [b],*, Luthais B. McCash [c], Haitham M.S. Bahaidarah [d], T. Aziz [e,f]

[a] *Department of Computer Science, Bahria University, Islamabad 44000, Pakistan*
[b] *Department of Electrical Engineering, Bahria University, Islamabad 44000, Pakistan*
[c] *Department of Mathematics, College of Science and Engineering University of Leicester, University Road, Leicester LE1 7RH, UK*
[d] *Department of Mechanical Engineering, King Fahd University of Petroleum and Minerals, Dhahran 31261, Saudi Arabia*
[e] *Department of Mathematics, Dammam Community College, King Fahd University of Petroleum and Minerals, KFUPM Box 5084, Dhahran 31261, Saudi Arabia*
[f] *Interdisciplinary Research Centre for Hydrogen and Energy Storage, King Fahd University of Petroleum and Minerals, Dhahran 31261, Saudi Arabia*

Abstract In this article, numerical simulation is performed for mixed convection lid-driven flow of *CuO*-water nanofluid enclosed in a curved corrugated. Cylindrical obstacles having three different constraints: (adiabatic, cold, and heated) at its surface are considered. Internal heat generation/absorption and uniform heat is provided at the vertical wall of the cavity. The bottom wall is insulated, and the curve surfaces are maintained with cold temperature. Mathematically equations are developed from physical problems and solved through Galerkin weighted residual method of FEM formulation. The effect of various Reynold number (Re), Darcy number (Da), solid volume fraction of nanoparticles (ϕ), heat generation/absorption coefficient (Q) and various cylindrical obstacle on velocity, Nusselt number, molecular movements and the flow structure has been studied. Nusselt number increases for high Darcy number due to the convection in lid cavity. For high Reynold number generally Nusselt numbers decrease or remain the same at the wall with an increase of nanoparticles in porous medium. There significant effect of heat sink coefficient on temperature profile and Nusselt number decreases with increasing of Q.

© 2021 THE AUTHORS. Published by Elsevier BV on behalf of Faculty of Engineering, Alexandria University. This is an open access article under the CC BY-NC-ND license (http://creativecommons.org/licenses/by-nc-nd/4.0/).

Nomenclature

x^*, y^*	Cartesian coordinates (m)	v	kinematic viscosity
u^*, v^*	velocities in the x & y directions (m/s)	α	thermal diffusivity
X^*, Y^*	dimensionless Cartesian coordinates	Gr	Grashof number
U^*, V^*	dimensionless velocities	H	characteristic length
Da	Darcy number	k	thermal conductivity
Re	Reynlod number	c_p	specific heat
Ri	Ricardson number	β	coefficients of thermal expension
Pr	Prandtl number	ψ	stream function
ϕ	volume fraction of nanoparticle	Q	heat generation and absropstion coefficent
ρ	density	m	shape of nanoparticles

1. Introduction

For decades, heat transfer in the cavity with a moving boundary in mixed convection is a fascinating phenomenon that has been worked on for engineers. The study of convection in a lid-driven cavity has attracted the perceptible attention of researchers due to numerous applications in the field of industrial microelectronics, nuclear power plant, food processing, renewable energy system etc. [1–6]. In addition to numerous engineering applications, it is of interest to analyse adverse conditions in which mixed convection heat transfer occurs as fundamental issues in transfer of heat and fluid flow. The influence of parameters such as Rayleigh number (Ra), Richardson number (Ri) and Grashof number on the overall Nusselt number will lead to better understanding and new applications in engineering featuring enhanced heat and mass transfer. Numerically, *Sivasankaran et al* [7] studied the influence of various nano-particles on the free convection of nanofluids in an enclosure. They noticed that the heat transfer enhancing significantly depends on the chosen nano-particles. Mixed convection flow in a low heated square driven cavity was numerically examined by *Moallemi and Jang* [8] and investigated the effect of Prandtl number on the flow and heat transfer mechanism. They found that the buoyancy effects are more prevailing for higher values of Prandtl number in a square lid driven enclosure. *Chamkha* [9] worked on the unsteady, mixed convection flow and heat transfer due to the heat generation/absorption fluid in a vertical lid driven cavity at uniform magnetic field. He summarized that the average Nusselt number decreases with an increase of internal heat generation coefficient but increases for the opposing flow. *Sivakumar et al* [10] analysed numerically the heat transfer and fluid flow of mixed convection in lid-driven cavities where the left vertical wall is partially heated. The variation of length and position of heated part of vertical wall is investigated and explores the transfer of heat and fluid flow in a cavity. On 3-dimensional structures, the numerical study was performed by *Ouertatani et al* [11]. They investigated the effect of double lid-driven (upper wall heated and lower cold). *Turkoglu and Yucel* [12] performed the analysis of mixed convection on inclined position with a presence of discrete heat source or element. They summarized that there is no significant effect on flow fluid due to the position of heated element or source.

In many situations, conventional cooling techniques involving the transfer of both free or force convection heat are not satisfactory. Enclosure preceding corrugated geometry is another specific type of attractive geometry and apposite, and finds usefulness in solar corrugated accumulator design and roof top design of houses. Porous substrates with high thermal conductivity are used in many applications such as industrial cooling equipment, heat interfaces or exchange, and solar collectors to improve forced-convection heat transfer. In view of the above work, [13–15] investigated the convection in porous medium and examined the heat transfer using a thermal non-equilibrium model. They analysed the effects of viscous and thermal dissipation porosity and inertial coefficient. *Sheikholeslami and Zeeshan* [16] performed the numerical approach to analyse the effects of volume fraction of nano-particles, Hartmann number (Ha) and buoyancy forces by means of CVFEM. Result demonstrates that with increasing Ha Nusselt number decrease but heat transfer increases as Ha varies but detracts against of buoyancy forces. *Sun et al.* [17] carried out analysis regarding the control of combined convection in a lid-driven cavity through triangular heated fins and noticed that the triangular fins in a cavity is a good parameter to control heat transfer and fluid. *Jeng and Tzeng* [18] investigated numerically convection in lid-driven cavity, filled with saturated water aluminium. They observed that Reynolds number directly effects the heat transfer in the cavity because of the mixed convection. *Shirvan et al* [19] examined the square cavity in mixed convection they analysed that Ha has reverse effect of heat transfer rate. The stable region in mixed convection lid driven cavity was identified by *Mohammad and Viskanta* [20]. Convection of heat transfer in different shaped cavity has been investigated in [21–26]. They worked on the tendency of heat transfer in various cavities with variant condition on walls. Several studies have been conducted to use nanoparticles, heat transfer and mixed convection wavy enclosure heat transfer and fluid flow characteristics [27–41].

After the brief literature review and to the best of the author's knowledge, it can be concluded that the present study of heat transfer rate and isotherm characteristics in mixed convection lid-driven curved corrugated porous cavity with inner cylindrical obstacle filled with CuO-water nano-fluid is one of the interesting topic to examine. That's why this article is to be analysed the effect of porous parameter, heat generation/absorption and different states of cylindrical obstacle. Graphically shows the interpretation of numerical results on core parameter, which has a greater impact on convection in cavity.

2. Problem formulation

Fig. 1 illustrates the curved corrugated of the two-dimensional porous lid-driven cavity examined in this article. The circular cylindrical obstacle inscribed inside enclosure. The nano-fluid is formed of base fluid (water) and copper solid spherical shape of nano-particles. The fluid is assumed to be laminar and incompressible. The bottom wall is thermally insulated $\left(\frac{\partial T^*}{\partial y^*} = 0\right)$, while the curved surface is sustained with low temperature T_c and left vertical wall with high temperature (T_H) to induce the buoyancy effect. Left vertical wall move with uniform velocity. H represents the characteristic length in horizontal and vertical direction in curved corrugated cavity.

Various constraints have been adjusted at cylinder (adiabatic, cold and hot) for observing the heat transfer within the enclosure.

2.1. Mathematical model

The governing equation for incompressible, Newtonian, laminar and steady state (thermal equilibrium) lid driven convection in a curve corrugated enclosure filled with a nano-fluid in the form of Navier-Stokes fomulation (mass, momentum and energy) written as;

$$\frac{\partial v^*}{\partial y^*} + \frac{\partial u^*}{\partial x^*} = 0, \tag{1}$$
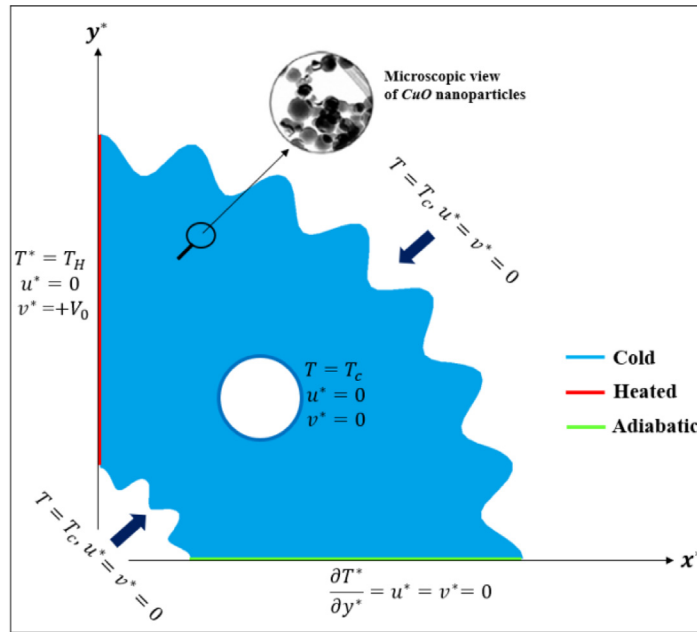
(a)
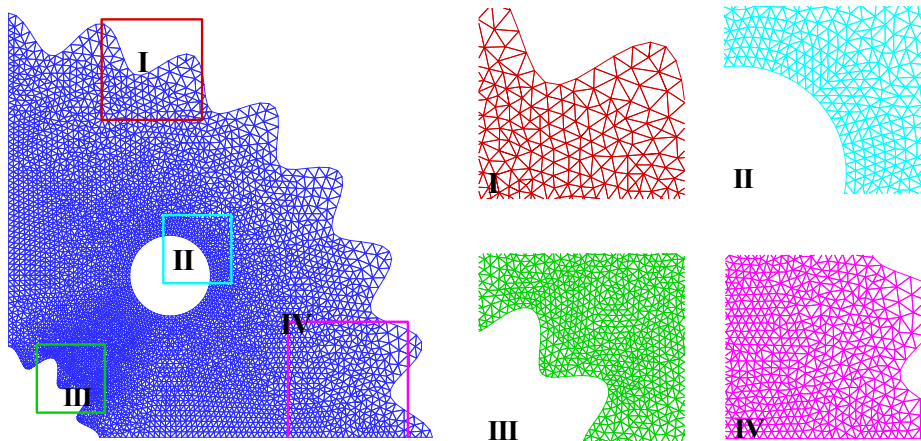
(b)

Fig. 1 Curved Corrugated geometry with its (a) physical domain (b) comutational domain with mesh distribution at various positions.

$$v^* \frac{\partial u^*}{\partial y^*} + u^* \frac{\partial u^*}{\partial x^*} = -\frac{1}{\rho_{nf}} \frac{\partial p^*}{\partial x^*} + v_{nf} \nabla^2 u^* - \frac{v_{nf}}{k} u^*, \tag{2}$$

$$v^* \frac{\partial v^*}{\partial y^*} + u^* \frac{\partial v^*}{\partial x^*} = -\frac{1}{\rho_{nf}} \frac{\partial p^*}{\partial y^*} + v_{nf} \nabla^2 v^* - \frac{v_{nf}}{k} v^* + \frac{(\rho\beta)_{nf}}{\rho_{nf}} g(T^* - T), \tag{3}$$

$$v^* \frac{\partial T^*}{\partial y^*} + u^* \frac{\partial T^*}{\partial x^*} = \alpha_{nf} \nabla^2 T^* + \frac{Q_0}{(\rho C_p)_{nf}} (T^* - T_c) \tag{4}$$

Where (u^*, v^*) are the velocity components along the (x^*, y^*), while T^*, p^* and g are the temperature, pressure and gravity acceleration respectively, ρ_{nf}, μ_{nf} and v_{nf} are the density, dynamic viscosity and kinematic viscosity respectively.

In the literature, several formulations are introduced for the thermo-physical properties of nanofluids. In this study we adopt the relationships which depend on the volume fraction of the nano-particles. The density of the nanofluid is given as:

$$\rho_{nf} = (1 - \phi)\rho_f + \phi\rho_p \tag{5}$$

Where ϕ is the solid volume fraction of the nanofluid, ρ_f and ρ_p are the densities of the fluid and of the solid frctions respectively, and the heat capacitance of the nanofluid given is by

$$(\rho C_p)_{nf} = (1 - \phi)(\rho C_p)_f + \phi(\rho C_p)_p \tag{6}$$

Thermal expansion coefficient of the nanofluid can be determined by:

$$(\rho\beta)_{nf} = (1 - \phi)(\rho\beta)_f + \phi(\rho\beta)_p \tag{7}$$

where β_f and β_p are the coefficients of the thermal expansion of the fluid and of the solid fractions respectively. Thermal diffusivity, α_{nf} of the nanofluid is defined as:

$$\alpha_{nf} = \frac{k_{nf}}{(\rho C_p)_{nf}} \tag{8}$$

For spherical nanoparticles thermal conductivity (k_{nf}) modeled by *Maxwell* [42] in Eq. (9) and in Eq. (10), μ_{nf} is dynamic viscosity of the nanofluid, given by *Brinkman* [43] are;

$$k_{nf} = k_f \left[\frac{k_s + (m-1)k_f - (m-1)\phi(k_f - k_s)}{k_s + (m-1)k_f + \phi(k_f - k_s)} \right] \tag{9}$$

$$\mu_{nf} = \mu_f(1 - \phi)^{-2.5} \tag{10}$$

Following dimensionless parameter are introduced;

$$(X^*, Y^*) = \left(\frac{x^*}{H}, \frac{y^*}{H} \right), \quad (U^*, V^*) = \left(\frac{u^*}{V_o}, \frac{v^*}{V_o} \right),$$

$$T^* = T_H + (T_H - T_c)\theta, \quad P = \frac{p^*}{\rho_{nf} V_o^2}, \quad Ri = \frac{Gr}{Re^2},$$

$$Q = \frac{Q_0 H^2}{(\rho C_p)_f \alpha_f}, \quad Pr = \frac{v_f}{\alpha_f} \tag{11}$$

into Eqns (1 – 4), the dimensionless form of equations become;

$$\frac{\partial V^*}{\partial Y^*} + \frac{\partial U^*}{\partial X^*} = 0, \tag{12}$$

$$\vec{V} \cdot \vec{\nabla} U^* = -\frac{\partial P}{\partial X^*} + \frac{1}{Re} \left(\frac{v_{nf}}{v_f} \right) \left(\nabla^2 U^* - \frac{U^*}{Da} \right), \tag{13}$$

$$\vec{V} \cdot \vec{\nabla} V^* = -\frac{\partial P}{\partial Y^*} + \frac{1}{Re} \left(\frac{v_{nf}}{v_f} \right) \left(\nabla^2 V^* - \frac{V^*}{Da} \right) + Ri \frac{(\rho\beta)_{nf}}{\rho_{nf}\beta_f} \theta, \tag{14}$$

$$\vec{V} \cdot \vec{\nabla} \theta = \left(\frac{\alpha_{nf}}{\alpha_f} \right) \left(\frac{1}{Pr Re} \right) \nabla^2 \theta + \left(\frac{Q}{Pr Re} \right) \frac{(\rho C_p)_f}{(\rho C_p)_{nf}} \theta. \tag{15}$$

2.2. Dimensionless boundary conditions:

a) At the bottom solid wall (Ω_1):

$$(U^*, V^*) = (0,0), \quad \frac{\partial \theta}{\partial Y^*} = 0, \tag{16}$$

b) At the upper curve surface (Ω_2):

$$(U^*, V^*) = (0,0), \quad \theta = 0, \tag{17}$$

c) At the left vertical wall (Ω_3):

$$(U^*, V^*) = (0,1), \quad \theta = 1, \tag{18}$$

d) At the lower curve surface (Ω_4):

$$(U^*, V^*) = (0,0), \quad \theta = 0, \tag{19}$$

e) At the surface of inner circle (Ω_5):

$$(U^*, V^*) = (0,0), \, and \, \left(\theta = 0 \, or \, \theta = 1 \, or \, \frac{\partial \theta}{\partial n_{\Omega_5}} = 0 \right), \tag{20}$$

The local Nusselt number for the heat transfer rate estimate are calculating using above equations;

$$Nu(Y^*) = -\frac{k_{nf}}{k_f} \left(\frac{\partial \theta}{\partial X^*} \right)_{X^*=0} \tag{21}$$

3. Methodology and comparison

The governed dimensionless Eqs. (13)–(16) along the boundary conditions are solved by Galerkin weighted residual finite element formulation. The domain is discritized in sub-domain and develop grid system of uniform meshes. By the weighted residue method convert the non-linear partial equations into system of integral equations, which is solved numerically. That integrals are solved through Gauss's quadrature method. These equation are transferred into non-linear algebraic equations by Newton Raphson technique iteration as already described by *Haq et al* [44] (see Tables 1-3).

To approximate the solution using the Newton Raphson technique iteratively. Using the relation of velocity in the form of stream function for fluid motion is follow:

Table 1 Values of shape factor for various shape of nano-particles.

Particle shapes	Spherical	Cylinder	Platelets	Brick
m	3	4.8	5.7	3.7

Table 2 Thermo-physical properties of Based fluid and Nanoparticles.

Physical properties	Base fluid (water)	*CuO*
C_p(J/kgK)	4179	540
ρ(kg/m^3)	997.1	6500
K(W/mK)	0.613	18
β (1/K)	2.1×10^{-4}	2.9×10^{-4}

Table 3 Average *Nu* numerical results comparison of present article, *Iwatsu et al* [1] and *Khanafer and Chamkha* [2] for a vertical gravity at $Ri = 0.01$.

Re	Present work	[1]	[2]
100	2.11	1.94	2.01
400	2.84	3.84	3.91
1000	6.27	6.33	6.33

$$U^* = \frac{\partial \psi}{\partial Y^*} ; V^* = -\frac{\partial \psi}{\partial X^*}. \qquad (22)$$
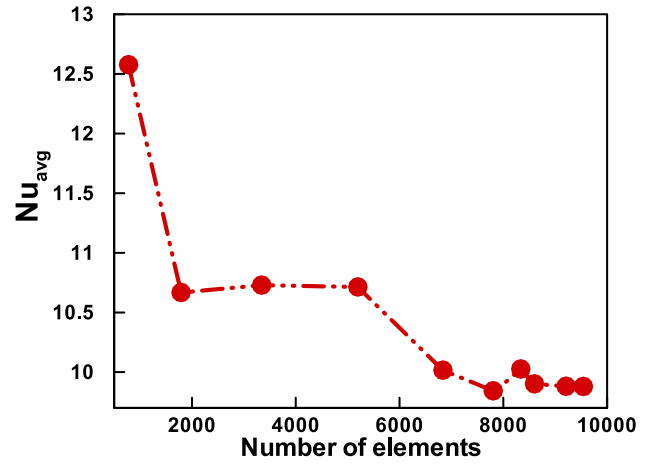
Fig. 2 Variation of average Nusselt number for various number of elements.

3.1. Grid independence

The study of various element against the average Nusselt number interpreted in Fig. 2. Variation of various number of element in enclosure does not significant effect on the average Nusselt number.

3.2. Comparison of result

In this section, we validate the computational result of present work with other manuscript. Mixed convection in lid-driven cavity problem compared to earlier findings by *Sivasankaran et al* [45] in Fig. 3(a), our present thermal contour analysis is depicted in Fig. 3(b). Excellent result validation of average
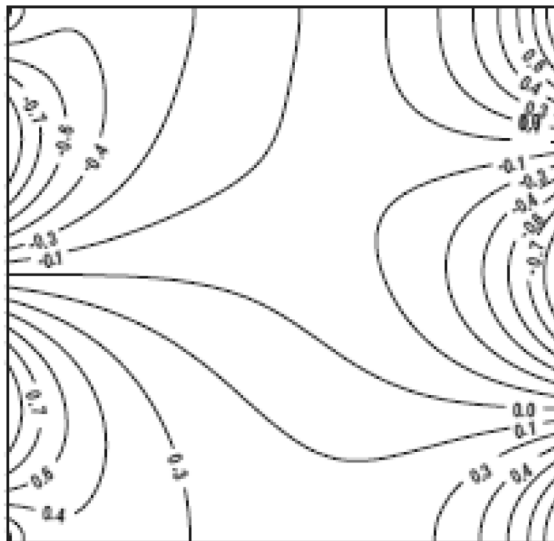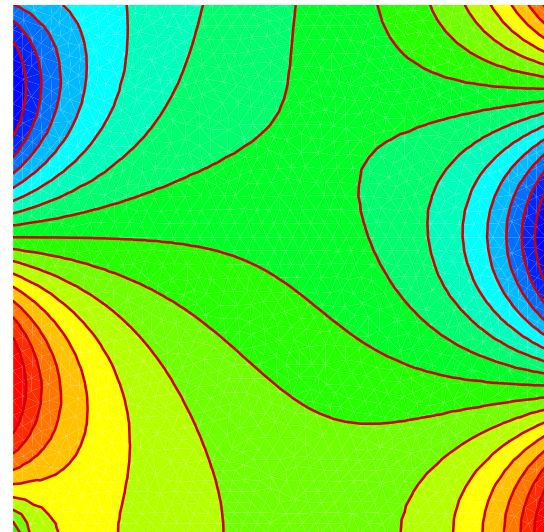
(a) *Sivasankaran et al*   (b) Present study

Fig. 3 Comparison of thermal contour analysis in a square cavity with sinusiodal boundary condition in limiting case: (a) *Sivasankaran et al* [45] versus (b) Present study.

Nusselt number against of different Re to the work of [1] and [2] in limiting case.

4. Results and discussion

A numerical work has been done in this article to study the flow structure and temperature profile for the various values of Reynold number $(100 \leq Re \leq 400)$, Darcy number $(Da = 10^{-5} to 10^{-1})$, nano-particle volume fraction $(0.0 \leq \phi \leq 0.05)$, heat generation/ absorption, Richardson number $(0.01 \leq Ri \leq 100)$ and different states of circular cylinder (adiabatic, cold and heated) inside of lid-driven cavity. Throughout the numerical computation Prandtl number $(Pr = 6.2)$ is fixed.
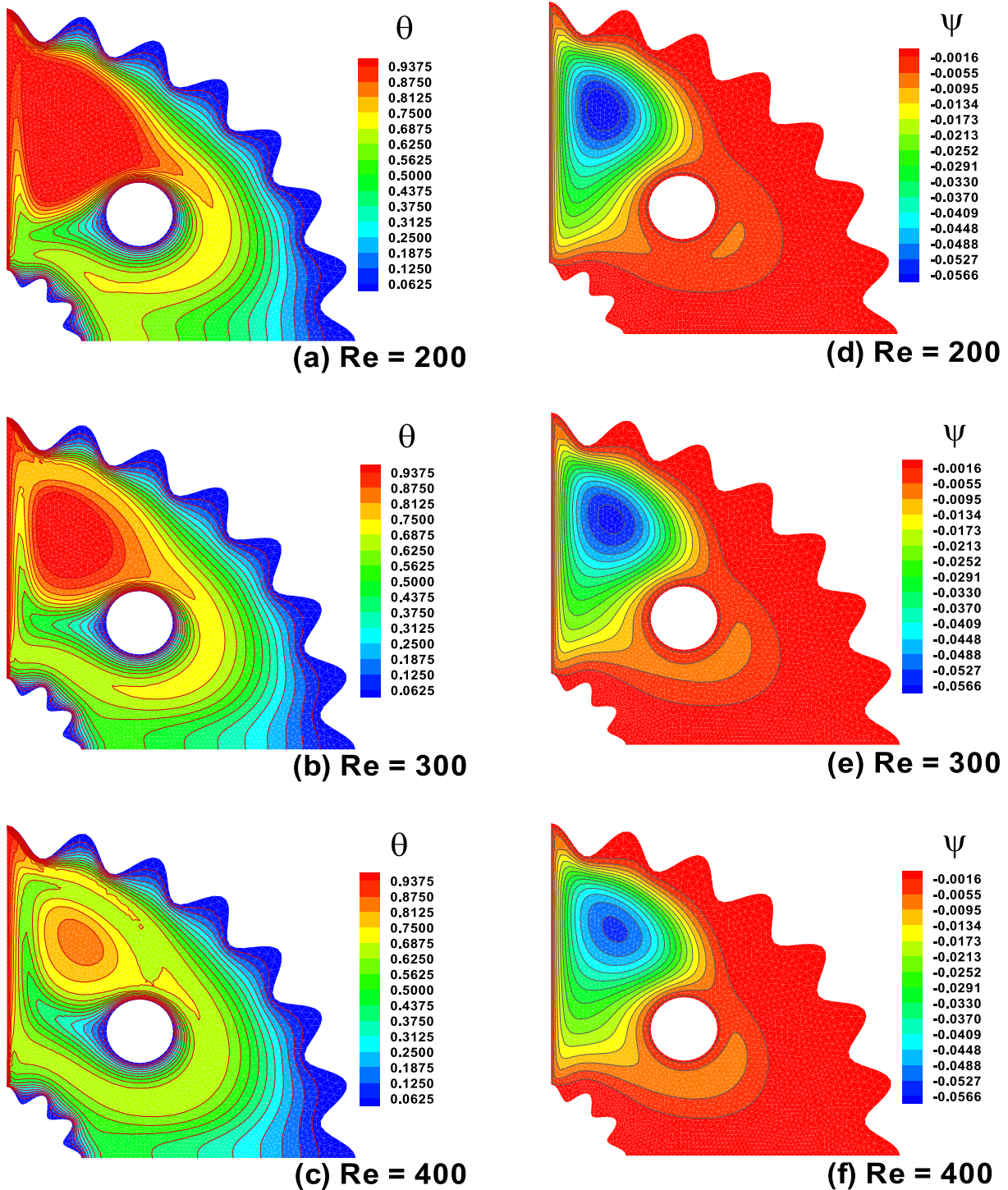
Fig. 4 Variation of (a)-(c) isotherm and (d)-(f) streamlines with respect to Re when $Ri = 0.01$, $Da = 10$, $\phi = 0.05$, $Q = 50$ for cold cylindrical obstacle.

4.1. Effect of Reynolds number

Fig. 4(a-f) describes the effect of Reynolds number on iso-therms and streamlines. It indicates that most of the cavity is filled by symmetrical undistorted isotherms, while the iso-therms endorse some form of distortion in a small part of the cavity neat to the top moving lid. For low Reynolds number, the isotherm is distributed on the whole enclosure, and gradually decreases with increasing *Re*. For maximum *Re* the heat effect around the moving heated vertical wall is shown in Fig. 4(c). Flow distribution for various number of *Re* can be seen in Fig. 4(d-f). For small Reynolds number, it can be noticed that the circular clockwise rotation of streamlines are developed. Small eddy is created, and with an increasing *Re*, the eddy move towards the center.

Fig. 5(a) represents the effect of horizontal velocity due to the variation of *Re*. It is clear that the velocity at centre increases with the increase of Reynolds number. For broader aspect, it is obvious that the center of the vortices lay smaller than near the corner of the cavity. Furthermore, it can be observed that the layers is established near the boundary along the solid wall as *Re* increases and heat swings from the solid boundary with a uniform vorticity. Fig. 5(b) indi-cates that velocity near the center decreases and create a nar-row boundary layer near the walls. Temperature profile at horizontal mean position is shown in Fig. 5(c). The average fluid temperature sharply decreases with an increasing of *Re*, due to volume fraction of nano-particles. Temperature also decreases in the cavity where the force convection is dominant. Nusselt number against heated vertical wall is illustrated in Fig. 5(d). In a cavity, convection increases *Nu*. It has significant impact on Nusselt number as Reynolds number increases.

4.2. Effect of nanoparticles

Fig. 6 illustrates the effect of nano-particle volume fraction on isotherm and streamlines. Thermal conductivity and viscosity
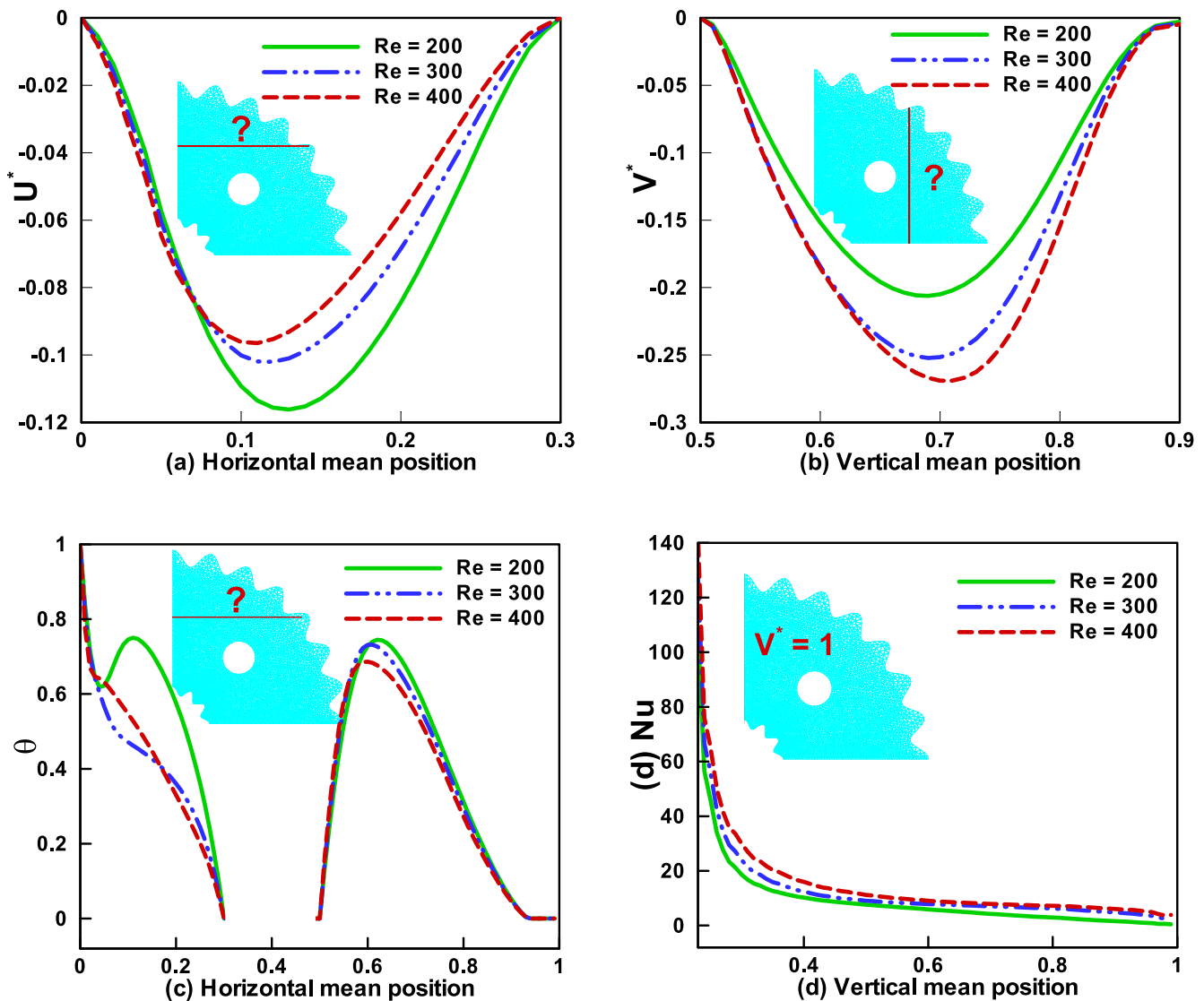
Fig. 5 Variation of (a) horizontal velocity, (b) vertical velocity, (c) Temperature and (d) Nusselt number with respect to *Re* for cold cylindrical obstacle.

(a) ϕ = 0.0

(d) ϕ = 0.0

(b) ϕ = 0.025

(e) ϕ = 0.025

(c) ϕ = 0.05

(f) ϕ = 0.05
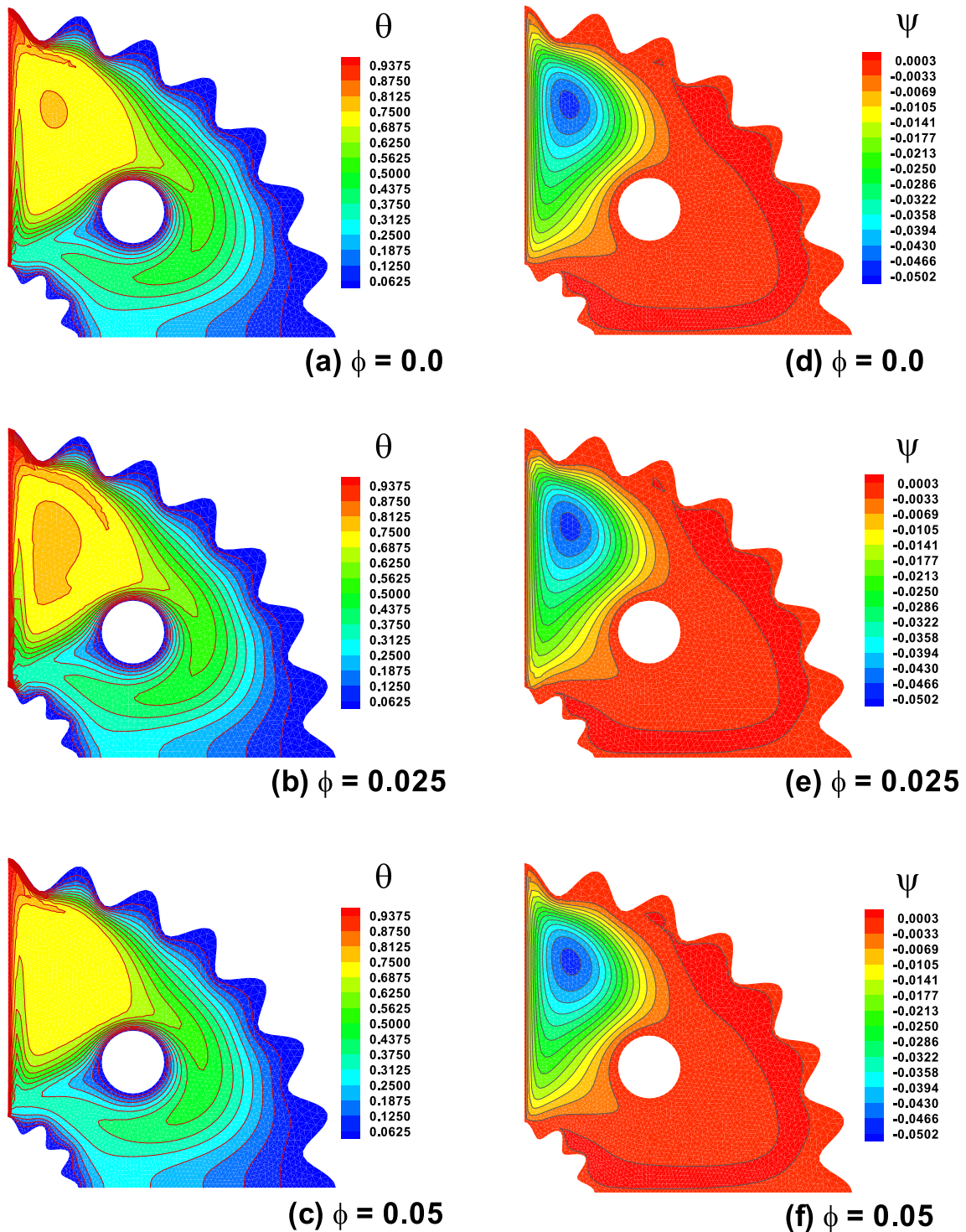
Fig. 6   Variation of (a)-(c) isotherm and (d)-(f) streamlines with respect to ϕ when $Ri = 0.01$, $Da = 0.01$, $Re = 350$, $Q = 10$ for cold cylindrical obstacle.

of fluid enhances when the nano-particles are mixed with base fluids. Fig. 6(a-c) describes the dominant nature of heat transfer of force convection, which occurs due to the heated mode of vertical lid moving with uniform velocity. Isotherm lines reveal that the prevailing heat transfer modes are force convection caused by the movement of vertical velocity. While the free convection is having a limited role in cavity due to the

nano-particles. Fig. 6(d-f) represents the streamlines for various values of nano-particles (ϕ). It can be clearly seen in the graph that at the top of circular cylinder, the eddy is developed due to the interacting of two bigger clockwise rotating roles which form a bigger eddy near the lid wall. With increasing of ϕ, the streamlines are more stronger around the circular surface of the cylindrical obstacle.
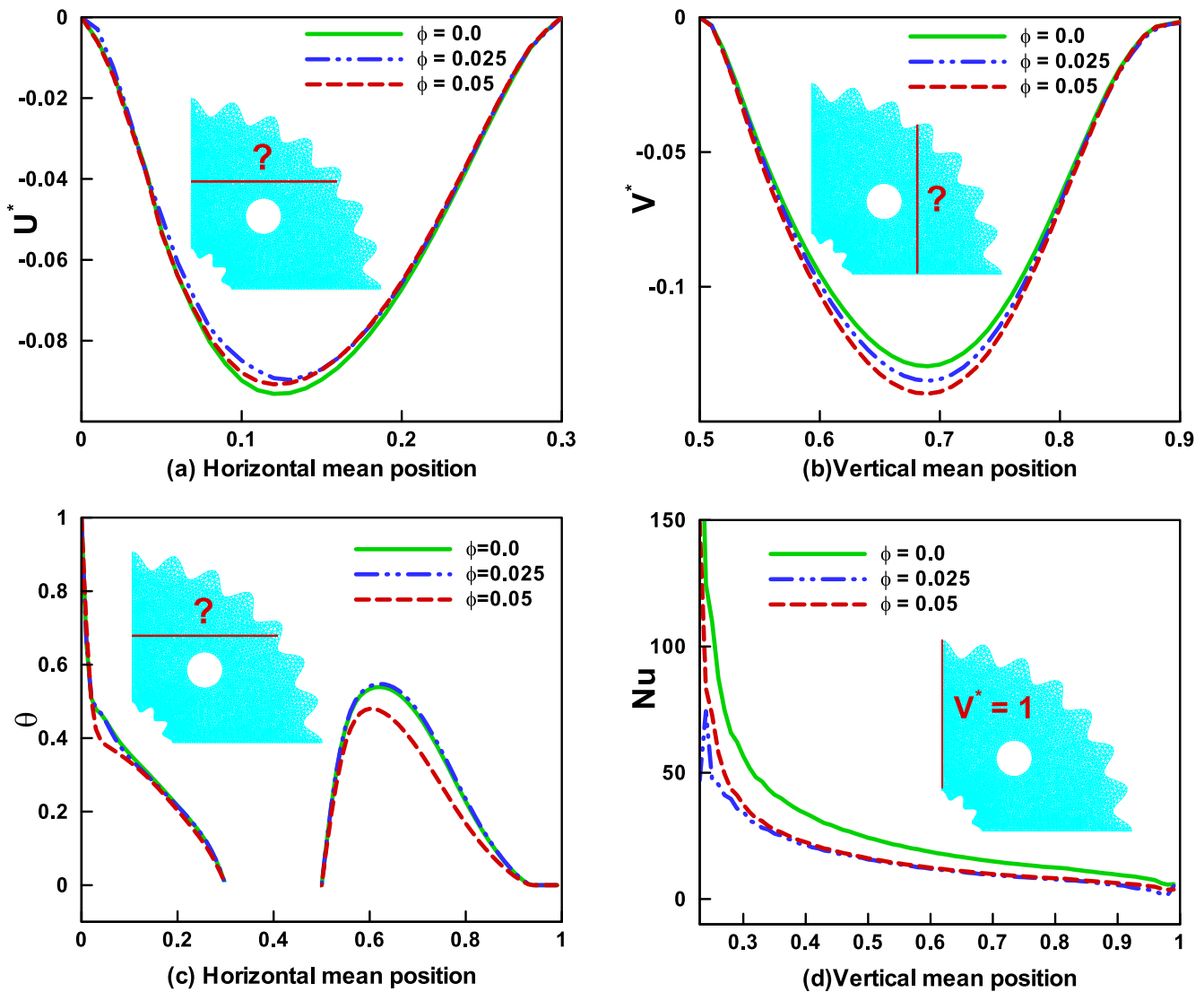
Fig. 7 Variation of (a) horizontal velocity, (b) vertical velocity, (c) Temperature and (d) Nusselt number with respect to ϕ for cold cylindrical obstacle.

In Fig. 7(a-f) illustrates the effect of nano-particles on the velocity, temperature profile and Nusselt number. Horizontal velocity increases with increasing volume fraction of nano-particles and attain its maximum position at the end points. But vertical velocity decreases with the increase of ϕ. Fig. 7 (c) represents the temperature distribution against the horizontal mean position. In case of base fluids $\phi = 0$, the cavity's temperature remains maximum at the end point but zero at the centre. While for $\phi = 0.1, 0.05$ temperature rapidly decreases due to the higher thermal conductivity of nano-particles and streamlines intensity decreases only significantly, as volume fraction increases, and temperature gradient decreases. With a reduction in temperature gradient with increasing volume fraction, there can be no specific estimation for the over all heat transfer within the cavity. As ϕ increases, nano-fluid thermal conductivity also enhances while marginally temperature gradient decreases. In a cavity, as heat transfer rate increases there will be enhancement in force convection

that can be clearly seen in Fig. 7(d) in the form of Nusselt number.

4.3. Effect of Richardson number

Fig. 8(a-h) show the isotherms and streamlines of assisting force flow for different values of Ri at the fixed value of Re. In isotherm the region affected by the heated vertical lid wall is quite small for small values of Ri and gradually increases with its increasing value. For higher value of Richardson number, the buoyancy effect are much stronger and more vigorous loops in the enclosure appeared in the figure. The intensity of the circulation in the form of bolus increases with the increase in Ri in the streamlines. At $Ri = 0.1$ the force convection dominants due to the vertical lid driven. However, at this value of Ri, the natural convection has been slightly affected at the corner which can almost be neglected. With the increase in $Ri = 1$ the mixed convection (inertial and buoyancy forces) balanced
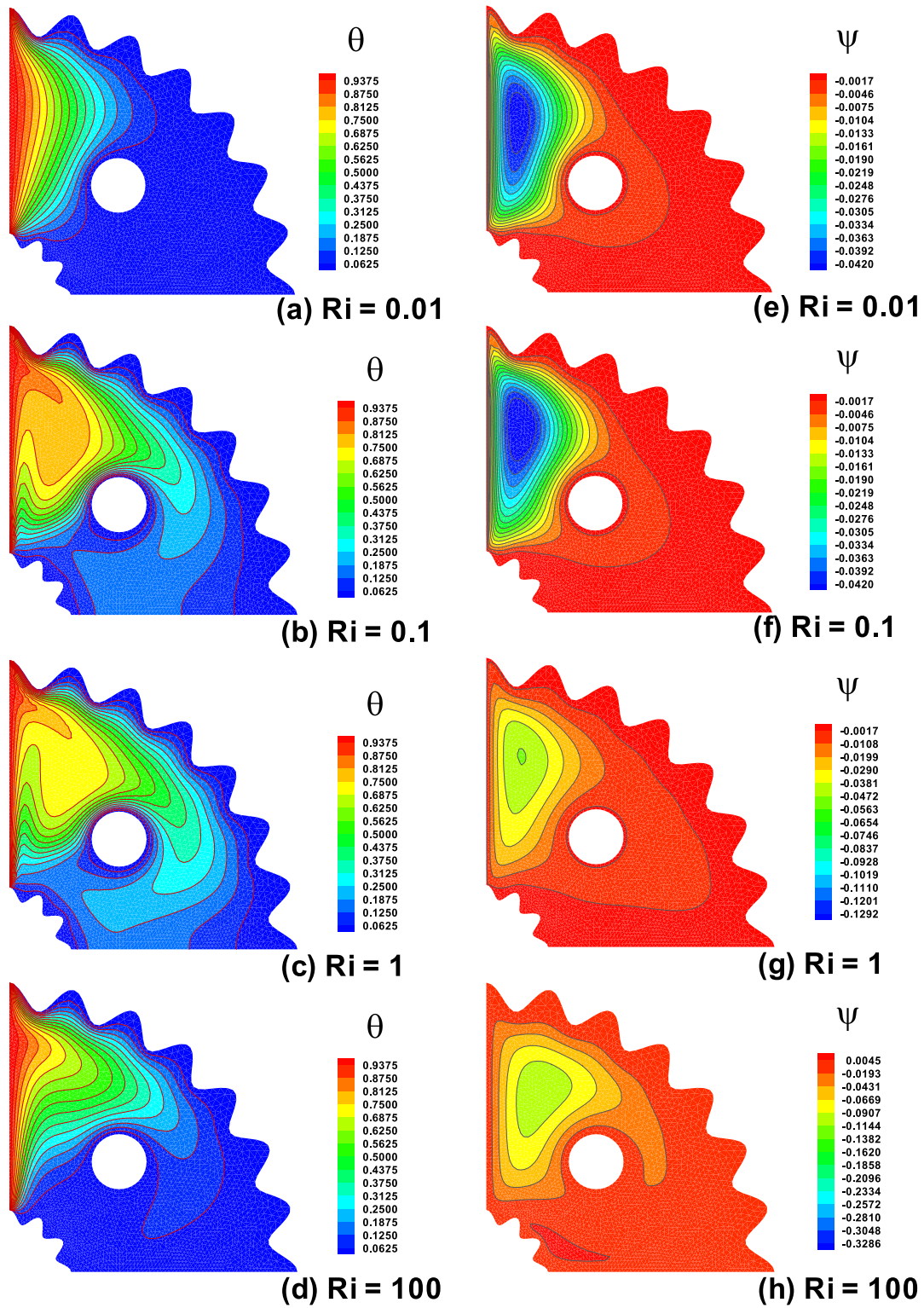
Fig. 8 Variation of (a)-(c) isotherm and (d)-(f) streamlines with respect to *Ri* when *Re* = 100, *Da* = 0.01, ϕ = 0.05, *Q* = 10 for cold cylindrical obstacle.
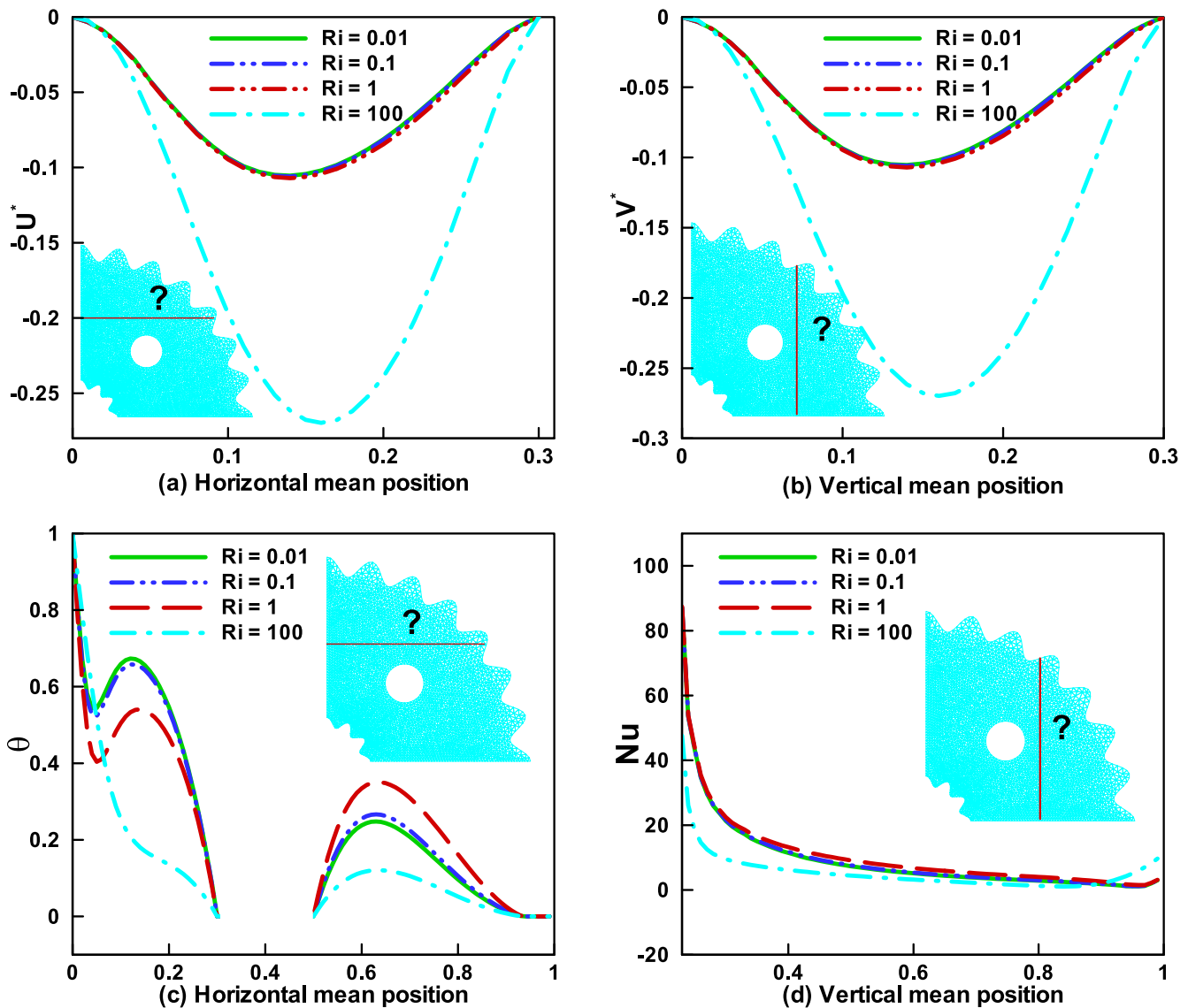
Fig. 9 Variation of (a) horizontal velocity, (b) vertical velocity, (c) Temperature and (d) Nusselt number with respect to *Ri* for cold cylindrical obstacle.

in the enclosure. At $Ri = 100$, the force convection decreases and buoyancy effect dominants as seen the Fig. 8(d).

Fig. 9(a-b) shows the variation of velocity against *Ri* horizontally and vertically. Here, velocity decreases with an increase in the values of *Ri* for both the cases. Force convection is dominants for the smaller values of *Ri* and increases with the larger values of *Ri* which turns to be natural convection as shown in Fig. 9(c). Local Nusselt number in the vertical mean position of the lid wall increases for the forced convection and decreases for natural convection.

4.4. Effect of porous medium

Fig. 10 illustrates the effect of Darcy number (porous medium) on isotherm and streamlines. The permeability in cavity have significant effect on heat transfer and flow of the molecular

movement. For a small number of $Da = 10^{-5}$ heat is located near the lid wall. For $Da = 10^{-3}$, as shown in Fig. 10(b), the convection of heat is raised and then heat is moved and created around the cooled circular surface of cylinder. Due to an increasing *Da*, heat transfer rate is increased. The convection is denominated with the increase of Darcy number. That's why temperature gradient moves towards the down surface where the conduction is dominant due to the minimal flow activities. Fig. 10(d-f) illustrates the result of different *Da* for maximum value of *Re*. For $Da = 10^{-5}$, the flow of lines are restricted near the vertical wall and for the recirculation small intensity of the flow of fluid. The stream lines for the recirculation flow region are elongation due to the increase of Darcy number. On the *Da*, the small eddy move towards downward direction to the centre point and the lines of stream are symmetric throughout the region.
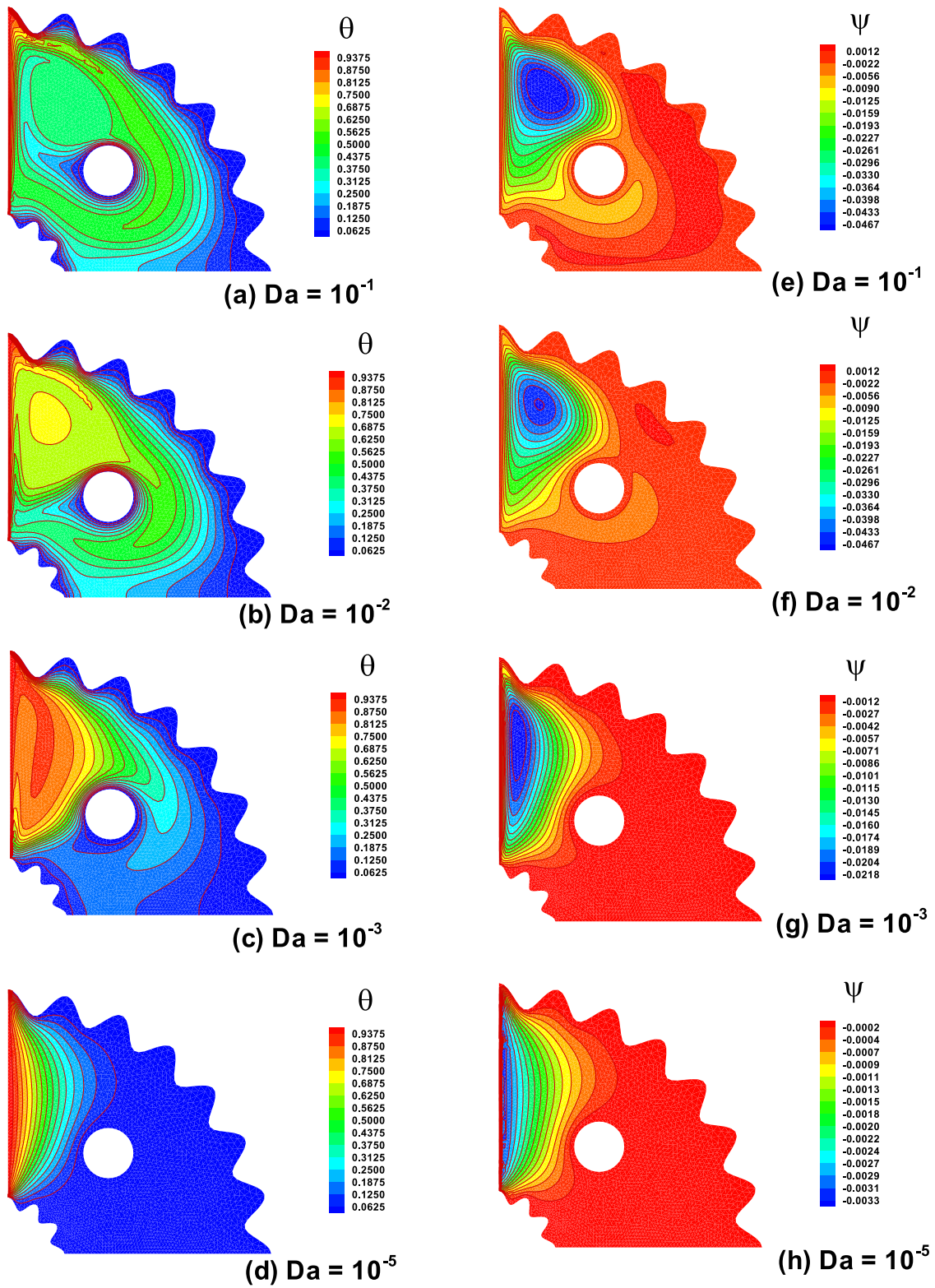
Fig. 10 Variation of (a)-(d) isotherm and (e)-(h) streamlines with respect to *Da* when *Ri* = 0.01, *ϕ* = 0.05, *Re* = 450, *Q* = 10 for cold cylindrical obstacle.
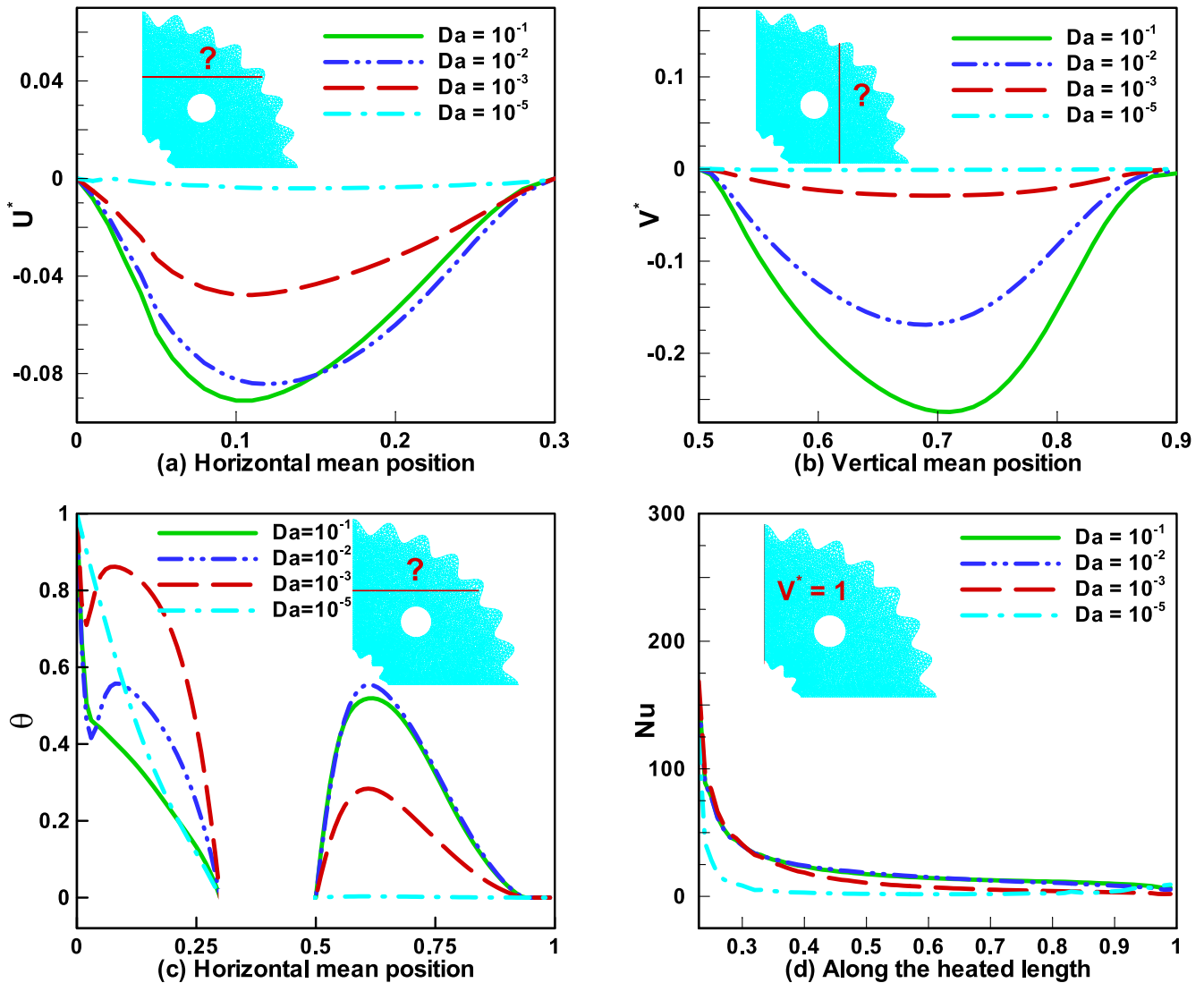
Fig. 11 Variation of (a) horizontal velocity, (b) vertical velocity, (c) Temperature and (d) Nusselt number with respect to *Da* for cold cylindrical obstacle.

Horizontal and vertical velocity related to various Darcy number is reported in Fig. 11. For greater value of *Da*, both velocities (horizontal and vertical) increases at the centre of the enclosure due to the greater convection for greater value of *Da*. For energy transportation, the inertial effects are retarded. For higher value of *Da*, the temperature slightly tilted down to the centre which is shown in Fig. 11(c). Temperature in cavity decreases due to the inertial coefficient which decreases with the increases porosity. Fig. 11(d) illustrates the effect of heat transfer. It can be observed in Fig. 11(d) that in the middle of cavity, the influence of *Da* will have a greater impact on *Nu* due to the convection. The transfer rate of heat are less near the right cold wall but higher near the heated wall for all *Da* values. It can be seen that the porous medium enhances the transformation, of energy in enclosure.

4.5. Effect of heat generation / absorption

Fig. 12 shows the effect of heat coefficient parameter *Q* on the molecular movement and streamlines in the curve cavity. It has significant role in energy equation. The variation in isotherm mostly appears due to the dependency on *Q* as it varies. $Q < 0$ represents the absorption of heat whereas, $Q > 0$ represents the internal heat generation. Near the closer area of the heated wall, the temperature effect becomes less as *Q* becomes smaller. Furthermore, it is due to the fact that the heat which is produced in this region increases both the domain temperature as well as the temperature gradient near the cold wall.

Fig. 13(c) illustrates that in case of heat generation ($Q > 0$), the temperature increases in cavity. The internal heating in energy equation represents the temperature rising near the ver-
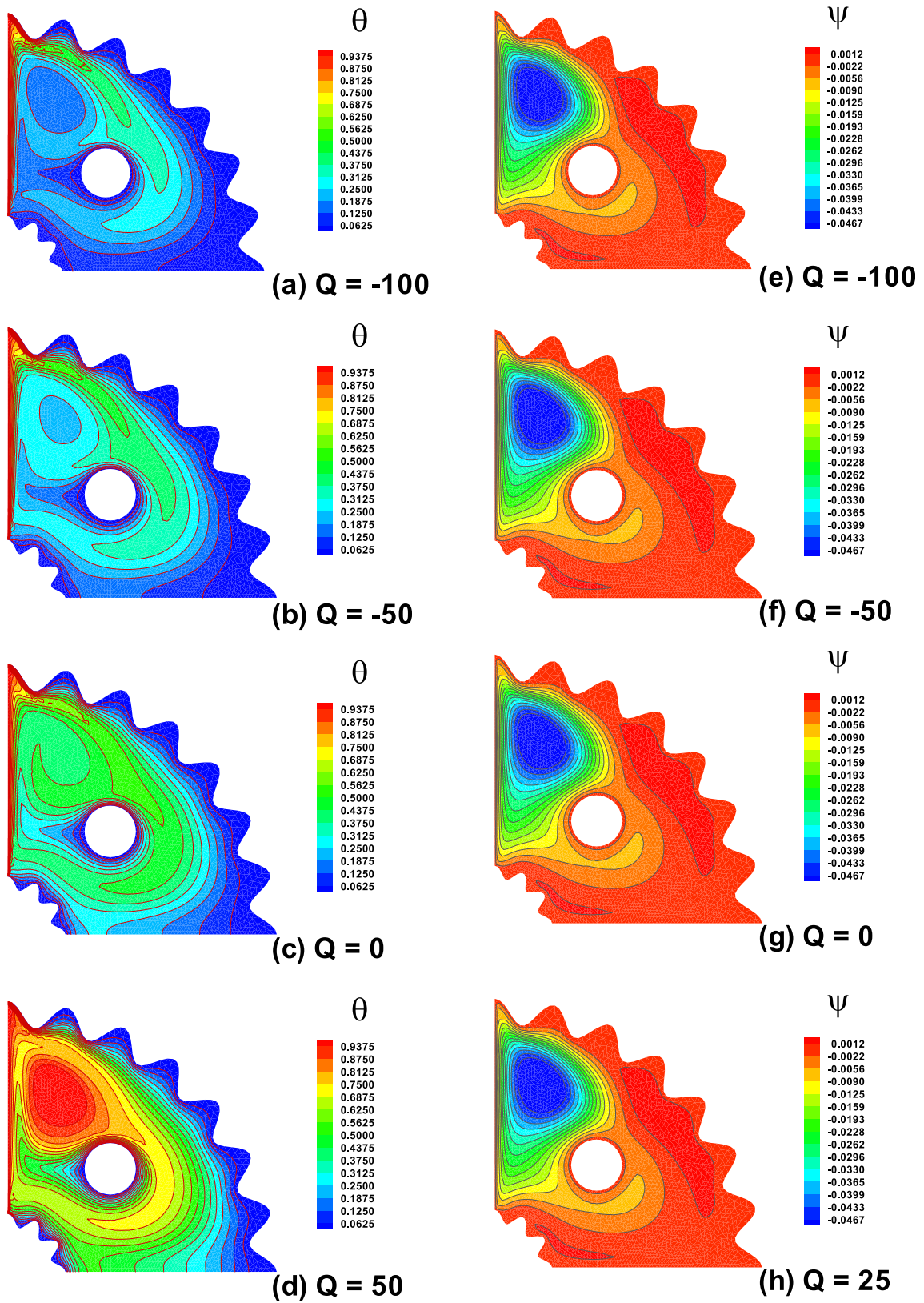
Fig. 12 Variation of (a)-(d) isotherm and (e)-(h) streamlines with respect to Q when $Ri = 0.01$, $\phi = 0.05$, $Re = 350$, $Da = 0.1$ for cold cylindrical obstacle.
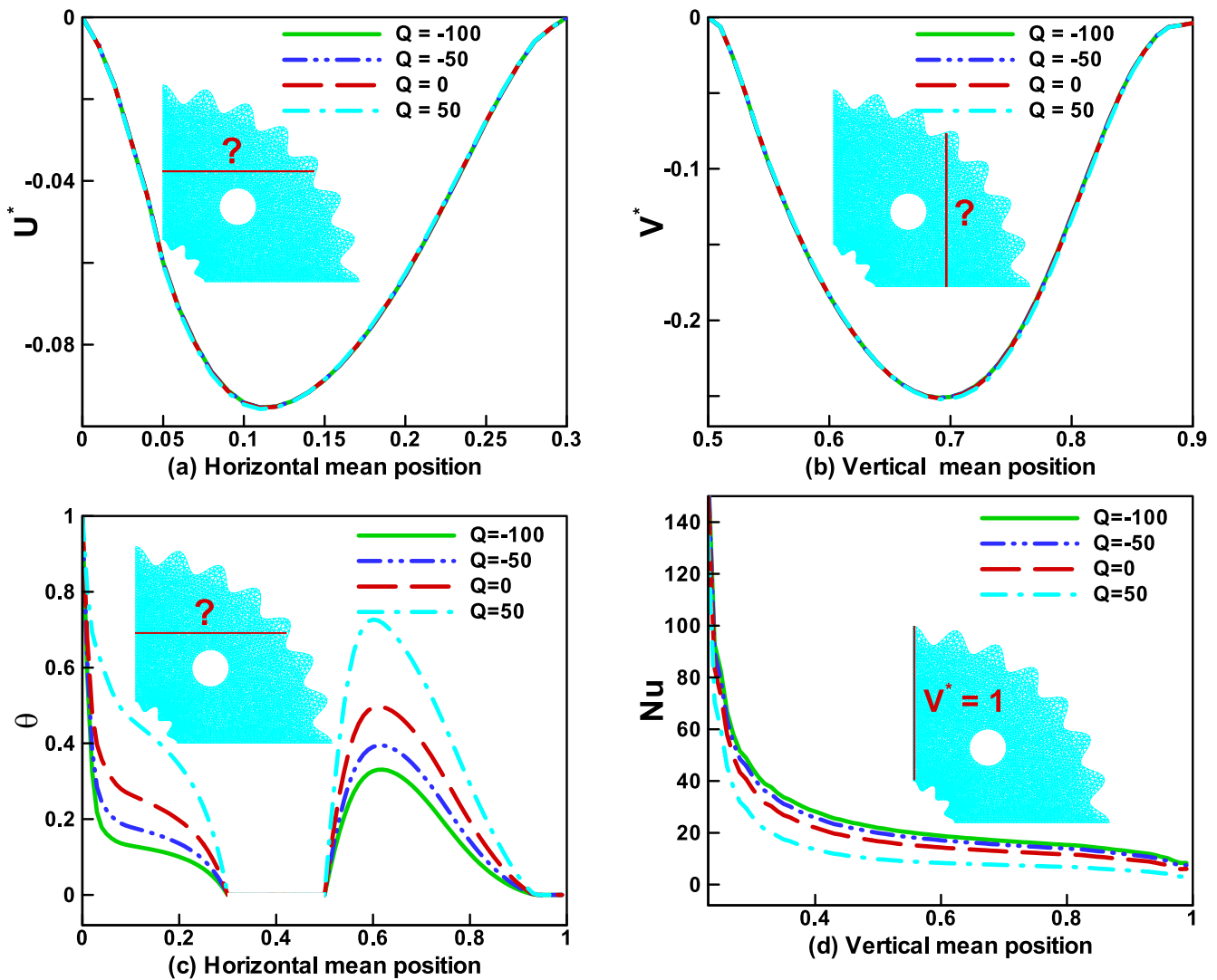
Fig. 13   Variation of (a) horizontal velocity, (b) vertical velocity, (c) Temperature and (d) Nusselt number with respect to Q for cold cylindrical obstacle.

tical wall specially. Due to the dominant role of heat generation in Nu, it decreases gradually as illustrated in Fig. 13(d).

4.6. Effect of different cylindrical surface

Isotherm and streamlines results due to the varies states (adiabatic, cold and heated) of circular cylinder as shown in Fig. 14. In cold and adiabatic case, the intensity of heat near the heated wall and circular surface is high and it gradually decreases towards the cold curve wall. Fig. 14(d-f) represents the variation of streamlines due to the varies state of cylinder. In each case, the same eddy is being created near the heated wall which results as the vertical wall moves and the movement of fluid particles is in clockwise direction. In adiabatic case, the streamlines spreads around the curve surface but in case of hot obstacle, the streamlines are away from the curve surface.

The effects on velocities, temperature and Nusselt number is shown in Fig. 15. The horizontal velocity is being measured from (0,0.3) as depicted in Fig. 15(a). It seems that the horizontal velocity is same near the heated vertical wall but is away from the wall which decreases in case of cold wall and increases in hot and adiabatic. Due to the hot surface, the velocity attain its maximum point it the middle of cavity. Fig. 15(c) represents the temperature at horizontal mean position. In case of a cold surface of cylinder, when the temperature from the heated wall moves towards the centre it gradually decreases at zero and for 0.25 it drops to zero. Where as, in case of the hot cylinder, when the temperature from the cylinder move towards the cold wall it attain its maximum point at 0.25. Temperature sharply increases in cavity and decreases in case of cold. Nusselt number decreases in heated curve surface and increase in cold case clearly seen in Fig. 15(d).
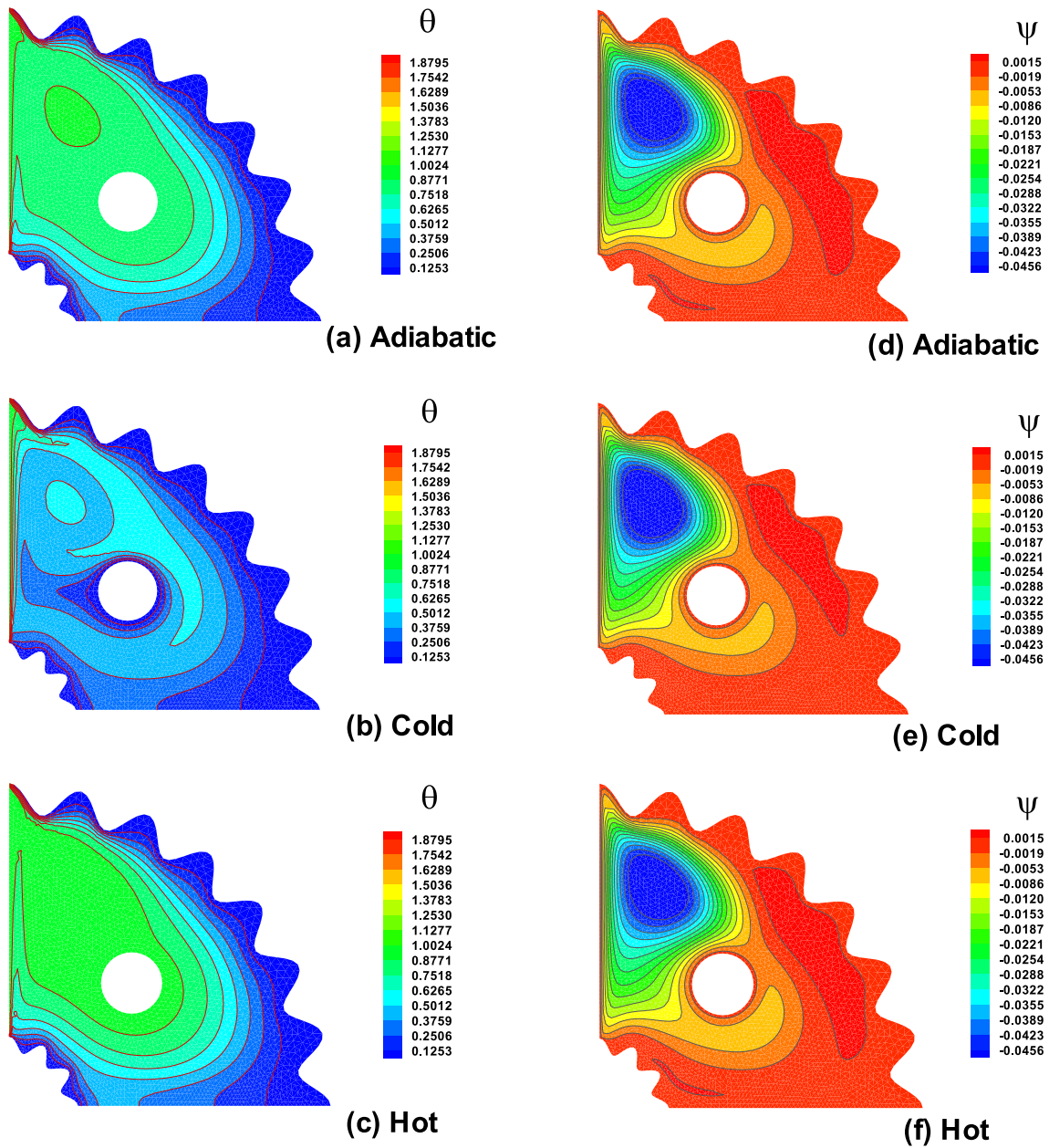
Fig. 14 Variation of (a)-(c) isotherm and (d)-(f) streamlines with respect to adiabatic, cold and hot cylindrical obstacle when $Ri = 0.01$, $\phi = 0.05$, $Re = 350$, $Da = 0.1$ $Q = 10$.

In Fig. 16(a) of an average Nusselt number, increasing the Reynolds number (Re) increases the Richardson number (Ri) due to the vertical heated lid wall. Fig. 16(b), depicts the minor increase in the average Nusselt number for smaller values of Darcy number with the increase in Re, whereas the minor increase of Nu_{avg} is observed against the higher values of Da with the same rate of Re.

Fig. 16(c) shows the effects of heat generation/absorption with respect to fixed Ri and various values of Re. It can be observed that increase in the internal heat absorption increases the convection of heat transfer. Whereas the increase in internal heat generation decreases the average Nusselt number. Fig. 16(d) depicts the variation of the average Nusselt number for various values of volume fraction and Reynolds number where it is seen that increasing the volume fraction causes the increase in the heat transfer for different values of Re.
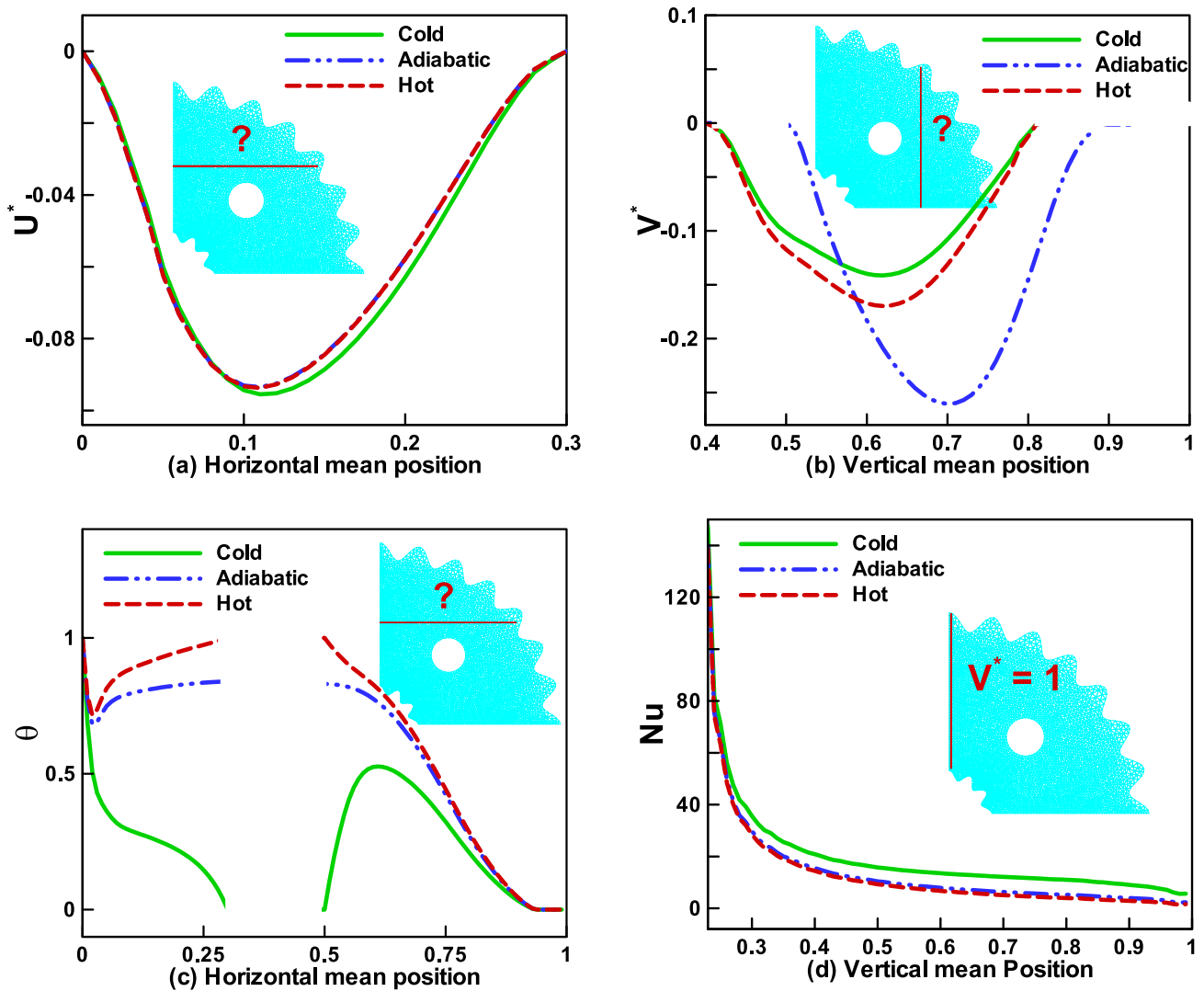
Fig. 15   Variation of (a) horizontal velocity, (b) vertical velocity, (c) Temperature and (d) Nusselt.

5. Conclusion

The effect of Reynold number $(100 \leq Re \leq 400)$, nano-particles $(0 \leq \phi \leq 0.05)$, Darcy number $(10^{-5} \leq Da \leq 0.1)$, absorption/generation parameter $(-100 \leq Q \leq 50)$ and different of cylindrical obstacle (adiabatic, cold and heated) on isotherm, streamline profile, temperature and Nusslet number were briefly discussed in this article. The study concluded with the following remarks:

- For a high Reynold number the force convection is dominant, so the heat transfer rate is high. Nusselt number increases with increase of Re.
- Small eddy created near the wall in streamlines due to the clockwise rotation of fluid.

- With increase of Re the symmetrical eddy moves toward the center of the cavity.
- Nanoparticles enhance the thermal conductivity of the fluid, so greater heat convection in cavity done when $\phi = 0.05$.
- Temperature distribution decreases near the heated wall with increases of Darcy number.
- Isotherm lines gradually limited around the heated vertical wall for high Darcy number.
- Temperature increases in case of heated cylindrical surface and Nusselt number decreases. Isotherm lines limited it the end face of heated wall in case of cold obstacle but isotherm lines are stronger in heated case.
- More heated generated in cavity for $Q > 0$. Temperature increases and Nusselt number decreases with increasing of heat sink parameter. Due to the heat generation isotherm lines are rapidly increases in enclosure.
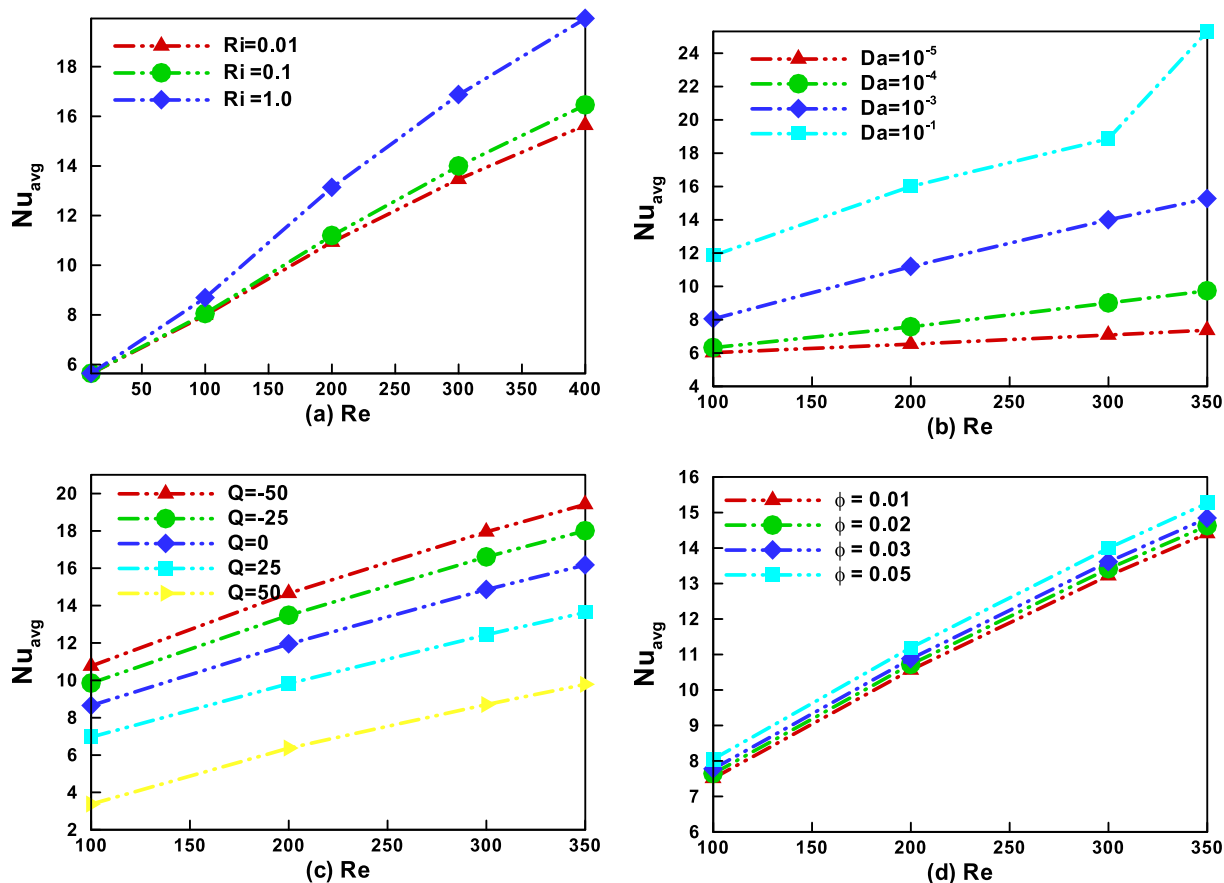
Fig. 16 Variation of average Nusselt number with respect to the Reynolds number at the different values of (a) Richardson number (b) Darcy number (c) Heat absorption/ generation coefficient (d) Volume fraction.

References

[1] R. Iwatsu, J.M. Hyun, K. Kuwahara, Mixed convection in a driven cavity with a stable vertical temperature gradient, Int. J. Heat Mass Transfer 36 (6) (1993) 1601–1608.

[2] K.M. Khanafer, A.J. Chamkha, Mixed convection flow in a lid-driven enclosure filled with a fluid-saturated porous medium, Int. J. Heat Mass Transfer 42 (13) (1999) 2465–2481.

[3] N. Alleborn, H. Raszillier, F. Durst, Lid-driven cavity with heat and mass transport, Int. J. Heat Mass Transfer 42 (5) (1999) 833–853.

[4] K. Khanafer, K. Vafai, Double-diffusive mixed convection in a lid-driven enclosure filled with a fluid-saturated porous medium, Numer. Heat Transfer, Part A 42 (2002) 465–486.

[5] K.M. Khanafer, A.M. Al-Amiri, I. Pop, Numerical simulation of unsteady mixed convection in a driven cavity using an externally excited sliding lid, Eur. J. Mech. B Fluids 26 (5) (2007) 669–687.

[6] A. Al-Amiri, K. Khanafer, J. Bull, I. Pop, Effect of sinusoidal wavy bottom surface on mixed convection heat transfer in a lid-driven cavity, Int. J. Heat Mass Transfer 50 (9-10) (2007) 1771–1780.

[7] S. Sivasankaran, T. Aasaithambi, S. Rajan, Natural Convection of Nanofluids in a Cavity with Linearly Varying Wall Temperature, Maejo Int. J. Sci. Technol. 4 (3) (2010) 468–482.

[8] M.K. Moallemi, K.S. Jang, Prandtl number effects on laminar mixed convection heat transfer in lid-driven cavity, Int. J. Heat Mass Transfer 35 (1992) 1881–1892.

[9] A.J. Chamkha, Hydromagnetic Combined Convection Flow in a Vertical Lid-Driven Cavity with Internal Heat Generation or Absorption, Numerical Heat Transfer, Part A 41 (5) (2002) 529–546.

[10] V. Sivakumar, S. Sivasankaran, P. Prakash, J. Lee, Effect of heating location and size on mixed convection in lid-driven cavities, Comput. Math. Appl. 59 (9) (2010) 3053–3065.

[11] N. Ouertatani, N.B. Cheikh, B.B. Beya, T. Lili, A. Campo, Mixed convection in a double lid-driven cubic cavity, Int. J. Therm. Sci. 48 (7) (2009) 1265–1272.

[12] H. Türkoĝlu, N. Yücel, Mixed Convection in Vertical Channels with a Discrete Heat SourceMischkonvektion in vertikalen Kanälen mit einer lokalen Wärmequelle, Heat Mass Transfer 30 (3) (1995) 159–166.

[13] K. Vafai, M. Sozen, Analysis of Energy and Momentum Transport for Fluid Flow through a Porous Bed, J. Heat Transfer 112 (1990) 690–699.

[14] A. Amiri, K. Vafai, Analysis of Dispersion Effects and Non-thermal Equilibrium, Non-Darcian, Variable Porosity Incompressible Flow through Porous Media, Int. J. Heat Mass Transfer 37 (6) (1994) 939–954.

[15] P.-X. Jiang, Z.-P. Ren, Numerical Investigation of Forced Convection Heat Transfer in Porous Media Using a Thermal Non-equilibrium Model, Int. J. Heat Fluid Flow 22 (1) (2001) 102–110.

[16] M. Sheikholeslami, A. Zeeshan, Analysis of flow and heat transfer in water based nanofluid due to magnetic field in a porous enclosure with constant heat flux using CVFEM, Comput. Methods Appl. Mech. Eng. 320 (2017) 68–81.

[17] C. Sun, B.o. Yu, H.F. Oztop, Y.i. Wang, J. Wei, Control of mixed convection in liddriven enclosures using conductive triangular fins, Int. J. Heat Mass Transfer 54 (4) (2011) 894–909.

[18] T.-M. Jeng, S.-C. Tzeng, Heat transfer in a lid-driven enclosure filled with water-saturated aluminum foams, Numerical Heat Transfer A 54 (2) (2008) 178–196.

[19] K.M. Shirvan, M. Mamourian, S. Mirzakhanlari, M. Moghiman, Investigation on effect of magnetic field on mixed convection heat transfer in a ventilated square cavity, Procedia Engineering 127 (2015) 1181–1188.

[20] A.A. Mohammad, R. Viskanta, Flow and heat transfer in a lid-driven cavity filled with stably stratified fluid, Applied Mathematical Modelling 19 (1995) 465–472.

[21] R.U. Haq, FerozAhmed Soomro, Toufik Mekkaoui, Qasem M. Al-Mdallal, MHD natural convection flow enclosure in a corrugated cavity filled with a porous medium, Int. J. Heat Mass Transf. 12 (9) (2018) 1168–1178.

[22] R.U. Haq, F.A. Soomro, Z. Hammouch, Heat transfer analysis of CuO-water enclosed in a partially heated rhombus with heated square obstacle, Int. J. Heat Mass Transf. 118 (2018) 773–784.

[23] M.M. Rahman, H.F. Öztop, R. Saidur, S. Mekhilef, K. Al-Salem, Finite element solution of MHD mixed convection in a channel with a fully or partially heated cavity, Comput. Fluids 79 (2013) 53–64.

[24] A.J. Chamkha, E. Abu-Nada, Mixed convection flow in a single and double lid driven square cavities filled with water-Al2O3nanofluid: effects of viscosity models, Eur. J. Mech. B-Fluid 36 (2012) 82–96.

[25] Seyyed Masoud Seyyedi, A.S. Dogonchi, M. Hashemi-Tilehnoee, Zeeshan Asghar, M. Waqas, D.D. Ganji, A computational framework for natural convective hydromagnetic flow via inclined cavity: an analysis subjected to entropy generation, J. Mol. Liq. 287 (2019) 110863, https://doi.org/10.1016/j.molliq.2019.04.140.

[26] E. Ghasemi, S. Soleimani, M. Bayat, Control volume based finite element method study of Nano-fluid natural convection heat transfer in an enclosure between a circular and a sinusoidal cylinder, Int. J. Nonlinear Sci. Numer. Simul. 14 (2013) 521–532, https://doi.org/10.1515/ijnsns-2012-0177.

[27] R.Md Kasmani, S. Sivasankaran, M. Bhuvaneswari, A.S. Alshomrani, Z. Soret and Dufour effects on doubly diffusive convection of nanofluid over a wedge in the presence of thermal radiation and suction, Scientia Iranica - Transaction B: Mech. Eng. 26 (5) (2019) 2817–2826.

[28] S. Sivasankaran, K. Narrein, Influence of Geometry and Magnetic Field on Convective Flow of Nanofluids in Trapezoidal Microchannel Heat Sink, Iranian Journal of Science and Technology - Transactions of Mechanical Engineering 44 (2020) 373–382.

[29] R.Md. Kasmani, S. Sivasankaran, M. Bhuvaneswari, A.H. Hussein, Analytical and numerical study on convection of nanofluid past a moving wedge with Soret and Dufour effects,

Int. J. Numerical Methods Heat and Fluid Flow 27 (10) (2017) 2333–2354.

[30] A.M. Rashad, S. Sivasankaran, M.A. Mansour, M. Bhuvaneswari, Magneto-convection of nanofluids in a lid-driven trapezoidal cavity with internal heat generation and discrete heating, Numerical Heat Transfer, Part A: Applications 71 (12) (2017) 1223–1234.

[31] S. Sivasankaran, M.A. Mansour, A.M. Rashad, M. Bhuvaneswari, MHD mixed convection of Cu-water nanofluid in a two-sided lid-driven porous cavity with a partial slip, Numerical Heat Transfer A 70 (12) (2016) 1356–1370.

[32] K. Narrein, S. Sivasankaran, P. Ganesan, Numerical investigation of two-phase laminar pulsating nanofluid flow in helical microchannel, Numerical Heat Transfer A 69 (8) (2016) 921–930.

[33] H.T. Cheong, S. Sivasankaran, M. Bhuvaneswari, Bhuvaneswari Effect of aspect ratio on natural convection in a porous wavy cavity, Arabian J. Science and Engineering 43 (3) (2018) 1409–1421.

[34] S. Sivasankaran, S.S. Ananthan, M. Bhuvaneswari, A.K.A. Hakeem, Double-diffusive mixed convection in a lid-driven cavity with non-uniform heating on sidewalls, Sadhana 42 (11) (2017) 1929–1941.

[35] S. Sivasankaran, S.S. Ananthan, M. Bhuvaneswari, A.K.A. Hakeem, Double-diffusive mixed convection in a lid-driven cavity with non-uniform heating on sidewalls, Sadhana 42 (11) (2017) 1929–1941.

[36] S. Sivasankaran, Kuo-Long Pan, Kuo-Long Pan Lattice Boltzmann simulation for a lid-driven cavity with discrete heating/cooling sources, AIAA Journal of Thermophysics and Heat Transfer 30 (3) (2016) 573–586.

[37] S. Sivasankaran, H.T. Cheong, M. Bhuvaneswari, P. Ganesan, Effect of Moving Wall Direction on Mixed Convection in an Inclined Lid-driven Square Cavity with Sinusoidal Heating, Numerical Heat Transfer A 69 (6) (2016) 630–642.

[38] S. Sivasankaran, V. Sivakumar, Ahmed Kadhim Hussein, P. Prakash, Prakash Mixed convection in a lid-driven two-dimensional square cavity with corner heating and internal heat generation, Numerical Heat Transfer A 65 (3) (2014) 269–286.

[39] Hao Guo, Kun Qian, Anjiang Cai, Jun Tang, Jun Liu, Ordered gold nanoparticle arrays on the tip of silver wrinkled structures for single molecule detection, Sensors and Actuators B: Chemical. 300 (2019) 126846, https://doi.org/10.1016/j.snb.2019.126846.

[40] Haiyan Yan, Xiuxiu Xue, Weixing Chen, Xinming Wu, Jingwei Dong, Yujun Liu, Zhao Wang, Reversible Na+ insertion/extraction in conductive polypyrrole-decorated *NaTi2(PO4)3* nanocomposite with outstanding electrochemical property, Applied Surface Science 530 (2020) 147295, https://doi.org/10.1016/j.apsusc.2020.147295.

[41] Zhang, Yongliang, Z. M. Liu, Zunmin, Research on heat transfer enhancement and flow characteristic of heat exchange surface in cosine style runner Heat and Mass Transfer, Vol 55 2019. 10.1007/s00231-019-02647-5.

[42] J. Maxwell, A Treatise on Electricity and Magnetism, Oxford University Press, Cambridge, UK, 1904.

[43] H.C. Brinkman, The Viscosity of Concentrated Suspensions and Solution, J. Chem. Phys. 20 (1952) 571–581.

[44] R.U. Haq, M. Usman, E.A. Algehyne, Natural convection of CuO-water nanofluid filled in a partially heated corrugated cavity: KKL model approach Communications in Theoretical, vol. 72, 8 2020.

[45] S. Sivasankaran, A. Malleswaran, Jinho Lee, Pon Sundar, Ganesan Hydro-magnetic combined convection in a lid-driven cavity with sinusoidal boundary conditions on both sidewalls, Int. J. Heat and Mass Transfer 54 (1-3) (2011) 512–525.